AIAA JOURNAL
Vol. 45, No. 4, April 2007

# Parametric Investigation of Gas Permeability in Cross-Ply Laminates Using Finite Elements

Jianlong Xu* and Bhavani V. Sankar†
*University of Florida, Gainesville, Florida 32611-6250*

DOI: 10.2514/1.26602

**Three-dimensional finite element models are used to study the influence of various parameters on the gas permeability of cross-ply composite laminate. It is shown that the intersection area, which is formed between two adjacent plies due to crack opening, is the most crucial factor in determining the permeability. It is found that the intersection areas obtained by superposing crack opening displacements of two-dimensional models are not accurate. A full three-dimensional model is required to obtain a detailed and precise prediction. The intersection area is found to be related not only to the resultant forces and thermal loads but also to the delamination shape and the delamination length. Laminates with different stacking sequence are studied, and it is found that for the same number of plies the laminate with dispersed plies shows lower permeability. Effect of temperature-dependent material properties is investigated as well.**

## Nomenclature

| | | |
|---|---|---|
| $a$ | = | delamination length |
| $B_0$ | = | permeability constant |
| $C$ | = | material constant related to permeability |
| $h$ | = | ply thickness |
| $M$ | = | molecular weight of gas |
| $N_x$, $N_y$ | = | force resultants |
| $p$ | = | gas pressure |
| $Q$ | = | volume flow rate |
| $R$ | = | universal gas constant |
| $T$ | = | temperature |
| $u$ | = | volume flow rate per unit area |
| $\Delta A$ | = | intersection area |
| $\Delta u$, $\Delta v$ | = | crack opening displacements |
| $\varepsilon_x$, $\varepsilon_y$ | = | strains |
| $\eta$ | = | viscosity of gas flow |
| $\lambda_i$ | = | crack density in $i$th ply |
| $\rho u$ | = | mass flow rate per unit area |

## I. Introduction

GRAPHITE/EPOXY composite laminates are considered as potential structural materials for future space vehicles, especially for the liquid hydrogen storage tank, due to its high strength/weight and high stiffness/weight ratio. A fundamental issue in using composite tank is hydrogen permeability. The liquid hydrogen storage tank at cryogenic temperature is subjected to large thermal and structural loads. This could cause matrix microcracking and subsequent delamination, which will form the gas leakage path. Understanding the mechanism of the hydrogen leakage through the composite laminates is very essential for successful use of composite laminates in cryogenic propellant tanks.

Many experimental studies have been conducted to measure the gas permeability in composite laminates. Based on ASTM standard D-1434 [1], Stokes [2] performed permeability testing on IM7/BMI laminated composites under biaxial strains. Nettles [3] tested permeability of composite laminate after impact testing. McManus et al. [4] investigated the influence of loading conditions, crack density, and ply orientation on the permeability of graphite/epoxy laminates. Choi [5] performed permeability tests on various composite material systems subjected to certain cryogenic cycles, and found that textile composite yields the lowest permeability. Kumazawa et al. [6] investigated helium gas leakage through composite laminates and compared the experimental results with the analytical models.

Several analytical models, such as initial shear lag analysis, interlaminar shear lag analysis, and variational approach, have been developed to investigate matrix microcracking and interlaminar delamination (see the review paper by Berthelot [7] and the references therein). Based on these analytical models, some researchers have modeled gas permeability in composite laminates [6,8]. The modeling is based on Darcy's law for porous media and the key point is to find the crack opening displacements in each ply, which will form the neck area in the gas leakage path. Kumazawa et al. [6] modeled gas leakage through composite laminates with transverse microcracking only, and their analysis was based on shear lag analysis. They assumed that mean crack opening displacement will form the gas leakage path. Theoretically, however, gas cannot leak through laminates without delamination. Roy and Benjamin [8] developed a model with delamination based on first-order shear deformable laminate theory and compared the analytical results with finite element results. Both of the aforementioned models are based on two-dimensional analysis and the crack opening displacements obtained from two-dimensional model are superposed to obtain the neck area in the gas leakage path.

In the present work, a three-dimensional analysis is performed to investigate the gas permeability through cross-ply composite laminates. Three-dimensional problems with delamination are so complicated that an analytical model is very hard or impossible to obtain. Therefore, finite element (FE) method will be adopted in the present analysis. It has been found that the local effects of delamination are quite significant and cannot be neglected. The effects of loading conditions, delamination length, and delamination shape on gas permeability are investigated in detail. The influences of temperature-dependent material properties and laminate layups are also investigated.

## II. Permeation Model

From experimental observations, matrix microcracking in 90-deg ply and interlaminar delamination between 0-deg ply and 90-deg ply are the first form of damage in composite laminates. The term

Presented as Paper 2093 at the 47th AIAA/ASME/ASCE/AHS/ASC Structures, Structural Dynamics & Materials Conference, Newport, RI, 1–4 May 2006; received 19 July 2006; accepted for publication 14 December 2006. 

*Graduate Student, Department of Mechanical and Aerospace Engineering, P.O. Box 116250; xujl@ufl.edu (corresponding author).

†Newton C. Ebaugh Professor, Department of Mechanical and Aerospace Engineering, P.O. Box 116250; Sankar@ufl.edu. Associate Fellow AIAA.

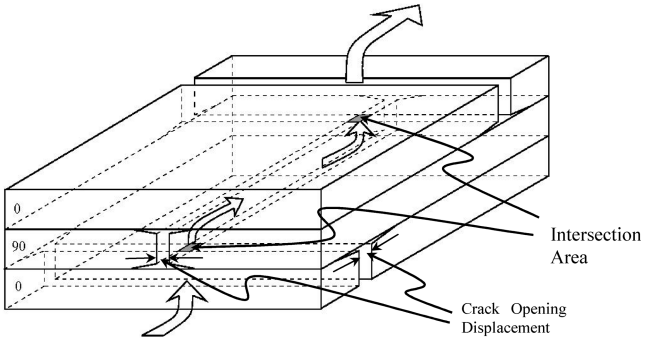


**Fig. 1 Gas permeation path through microcracks in cross-ply laminates.**

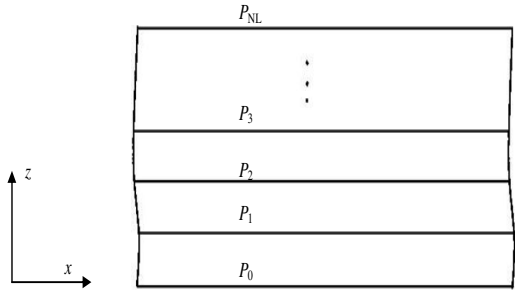


**Fig. 2 Gas pressure distribution across the laminate. $P_0$ ($P_b$) and $P_{NL}$ ($P_t$) represent the pressure at the bottom and the top of laminate, respectively, and $P_1$ to $P_{NL-1}$ represent pressures at the interfaces.**

"microcrack" used in the current model refers to the transverse crack in 90-deg ply fully developed through ply thickness and fully propagated across the laminate width. Theoretically, microcracks alone cannot form a contiguous path for gas leakage. Hence the delamination has to be introduced in the numerical model as shown in Fig. 1. The shaded intersection areas are formed by the crack opening displacements (CODs), which are the crack opening of the transverse microcracks measured at the ply interface, as shown in Fig. 1. These intersection areas connect the microcracks to form the pathways for the cryogenic gas.

The permeability modeling is based on Darcy's law for porous material [8]. Darcy's law for isothermal, viscous flow of gases through porous media is given as

$$\rho u = -\frac{B_0 M p}{\eta R T}\frac{\mathrm{d}p}{\mathrm{d}x} \tag{1}$$

Integration of Eq. (1) through the thickness of the composite laminate yields

$$\rho u h^{(\mathrm{Total})} = -\frac{B_0 M}{\eta R T}\frac{p_t^2 - p_b^2}{2} \tag{2}$$

where $h^{(\mathrm{Total})}$ is the thickness of laminate, $p_t$ and $p_b$ are pressures at top and bottom of laminate, respectively.

At the same time, if the integration is performed in individual layers (see Fig. 2), similar equation for each lamina can be obtained as

$$\rho u h^{(i)} = -\frac{B_0^{(i)} M}{\eta R T}\frac{p_i^2 - p_{i-1}^2}{2}, \qquad i = 1, 2, \ldots, \mathrm{NL} \tag{3}$$

where $h^{(i)}$, $B_0^{(i)}$, and $p_i$ are thickness, permeability constant, and gas pressure of $i$th lamina, respectively, and NL is the number of laminas. Obviously, $p_0 = p_b$ and $p_{\mathrm{NL}} = p_t$.

From Eq. (3), one can obtain

$$p_i^2 - p_{i-1}^2 = -\frac{2\rho u \eta R T}{M}\frac{h^{(i)}}{B_0^{(i)}} \tag{4}$$

Summing the preceding equation from $i = 1$ to $i = \mathrm{NL}$ yields

$$p_{\mathrm{NL}}^2 - p_0^2 = -\frac{2\rho u \eta R T}{M}\sum_{i=1}^{\mathrm{NL}}\frac{h^{(i)}}{B_0^{(i)}} \tag{5}$$

Comparing Eq. (5) with Eq. (2), it can be seen that

$$B_0 = \frac{h^{(\mathrm{Total})}}{\sum_{i=1}^{\mathrm{NL}}\frac{h^{(i)}}{B_0^{(i)}}} \tag{6}$$

Once a laminate is given, the permeability constant $B_0$ is determined by the thickness and the permeability of each ply. To get the $B_0^{(i)}$ for each ply, we consider the Poiseuille law for laminar flow through a capillary [9]:

$$Q = \frac{\pi d^4 \Delta P}{128 \eta L} \tag{7}$$

where $Q$ is volume flow rate, $d$ is inner diameter of the capillary, $\Delta P$ is pressure drop along the capillary, and $L$ is length of capillary. Dividing both sides of Eq. (7) by the cross-sectional area of capillary, the volume flow rate per unit area is given by

$$u = \frac{d^2 \Delta P}{32 \eta L} \tag{8}$$

Comparing Eq. (8) with Eq. (1), it can be seen that for a capillary, the permeability constant is proportional to $d^2$, or the cross-sectional area of the capillary. Based on this fact, we can assume the permeability constant for each intersection area is proportional to the area. The number of intersection areas can be determined by the crack densities of adjacent plies. So the permeability for the ply is assumed to be proportional to the total intersection area of the ply under consideration. Note that a laminate with NL plies will have (NL − 1) interfaces. Each of the inner plies has two interfaces with adjacent plies, so the intersection area is taken as the average of the areas at two interfaces. The first and last plies only have one interface with adjacent plies, so the intersection area at that interface is used for those plies. Hence the permeability of each ply is assumed to take following form:

$$\begin{aligned} B_0^{(1)} &= C\lambda_1\lambda_2\Delta A^{(1,2)} \quad \text{for } i = 2, \ldots, \mathrm{NL}-1 \\ B_0^{(i)} &= \frac{1}{2}C(\lambda_{i-1}\lambda_i\Delta A^{(i-1,i)} + \lambda_i\lambda_{i+1}\Delta A^{(i,i+1)}) \\ B_0^{(\mathrm{NL})} &= C\lambda_{\mathrm{NL}-1}\lambda_{\mathrm{NL}}\Delta A^{(\mathrm{NL}-1,\mathrm{NL})} \end{aligned} \tag{9}$$

where $C$ is material property which can only be determined from experiments [4] and $\Delta A^{(i,j)}$ is the intersection area at interface between $i$th and $j$th plies as shown in Fig. 1. Hence, Eq. (6) can be rewritten as

$$B_0 = C\frac{h^{(\mathrm{Total})}}{(h^{(1)}/\lambda_1\lambda_2\Delta A^{(1,2)}) + \sum_{i=2}^{\mathrm{NL}-1}[2h^{(i)}/(\lambda_{i-1}\lambda_i\Delta A^{(i-1,i)} + \lambda_i\lambda_{i+1}\Delta A^{(i,i+1)})] + (h^{(\mathrm{NL})}/\lambda_{\mathrm{NL}-1}\lambda_{\mathrm{NL}}\Delta A^{(\mathrm{NL}-1,\mathrm{NL})})} \tag{10}$$

**Table 1 Orthotropic material properties for the composite: $E$, $G$, $\nu$, and $\alpha$, respectively, are the Young's modulus, shear modulus, Poisson's ratio, and coefficient of thermal expansion. Elastic moduli are in GPa.**

| Property | Value |
|---|---|
| $E_1$ | 169 |
| $E_2$ | 8.62 |
| $E_3$ | 8.62 |
| $\nu_{12}$ | 0.355 |
| $\nu_{13}$ | 0.355 |
| $\nu_{23}$ | 0.410 |
| $G_{12}$ | 5.0 |
| $G_{13}$ | 5.0 |
| $G_{23}$ | 1.22 |
| $\alpha_1$ | $-0.003384e^{-6}/°C$ |
| $\alpha_2$ | $28.998e^{-6}/°C$ |
| $\alpha_3$ | $28.998e^{-6}/°C$ |

It is obvious from Eq. (10) that the permeability is determined by the crack densities $\lambda_i$ and the intersection areas $\Delta A^{(i,j)}$ once the material constant $C$ is characterized by experiments. Bapanapalli et al. [10] has developed a method based on FE modeling to determine the crack densities in cross-ply laminates subjected to biaxial and thermal loading. Hence, in this paper, we mainly focus on determining the intersection area $\Delta A^{(i,j)}$. In the present work, symmetric cross-ply laminates [0/90/0] subjected to biaxial and thermal loading are investigated. The orthotropic material properties are shown in Table 1 [10]. The ply thickness $h$ is taken as 0.33 mm.

## III. Two-Dimensional FE Modeling

Before using a fully three-dimensional finite element model, two-dimensional FE modeling is presented first to find the proper delamination length. Figure 3 shows two different cases of delamination. In the first case, [90/0/90], the delamination emanates from the surface ply of the laminate whereas in the second case, [0/90/0], it emanates from the middle ply. Because of symmetry, only one fourth of the unit cell is considered in the simulation. The crack densities are taken as 1 $cm^{-1}$.

The simulation has been done using the commercial FE software ABAQUS 6.5™. In this investigation, eight-node plane strain isoparametric elements and uniform meshes are used. A total of 15,600 elements are generated. Even though the individual mode 1 and mode 2 strain-energy release rates do not exist due to the oscillatory characteristic of stresses and displacements near the crack tip for bimaterial interface cracks [11], the total strain-energy release rate is well defined. Under linear elastic assumption, path independent J-integral is identical to the strain-energy release rate. Because J-integral is insensitive to the finite element method (FEM) mesh, uniform mesh is accurate enough for this simulation.

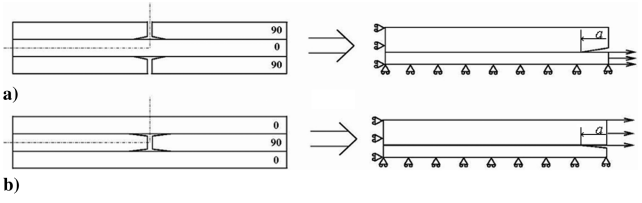


**Fig. 3 Two-dimensional delamination model: a) delamination from surface plies [90/0/90]; b) delamination from middle ply [0/90/0].**

The J-integrals with respect to the delamination length are computed as shown in Fig. 4. The delamination length is normalized by the ply thickness in Fig. 4. The unit cell is under constant displacement loading. It can be seen that the J-integral reaches maximum value when delamination length is about the ply thickness, and then decreases slowly. This implies that the delamination propagate steadily when delamination length exceeds ply thickness under displacement control loading. When the delamination length is too small, less than the ply thickness, the boundary effects are quite obvious.

From Fig. 4, it seems to be a proper choice to take ply thickness as the delamination length because the delamination propagates steadily after its length exceeds ply thickness. Hence, in the following three-dimensional FE analysis, a length comparable to the ply thickness is taken to be the delamination length and the sensitivity of the intersection area to the delamination length is investigated.

## IV. Three-Dimensional FE modeling

### A. Model Description

Once the crack densities are determined, the dimensions of the unit cell are fixed as shown in Fig. 5. In the present model, the crack densities in the 0- and 90-deg plies are taken as equal, $\lambda_x = \lambda_y = 1$ $cm^{-1}$. In this case, the factor that determines the permeability is the intersection area $\Delta A$ [see Eq. (10)]. Hence in three-dimensional modeling, most attention will be paid to computing the intersection area. The material properties and ply thickness are kept identical to those of the two-dimensional model.

Because of both in-plane symmetry and symmetry in thickness direction, only one eighth of the unit cell is analyzed. As shown in Fig. 5a, the two free surfaces are the microcrack faces; symmetric boundary conditions are applied to the surfaces opposite to the free surfaces and bottom surface, constant strains are applied as shown by the arrows, and the delaminations emanated from both surface ply and middle ply form a rectangle delamination front. Twenty-node 3-D isoparametric solid elements and uniform mesh are used in the simulation. A total of 28,224 elements are generated in the present model. Figure 5b shows a typical deformation of the model under biaxial loading. Note that the deformation is enlarged by a factor of 10.

Kumazawa et al. [6] and Roy and Benjamin [8] proposed superposition of two-dimensional CODs to get the intersection area. In fact, if one monitors the COD along the path shown by the arrow in Fig. 6a, the COD, normalized by the ply thickness, first remains constant along the straight edge, and then increases remarkably as it gets close to the rectangular crack front. The constant value is identical to the result predicted by two-dimensional model. The COD near the rectangular delamination front, however, is almost 50%

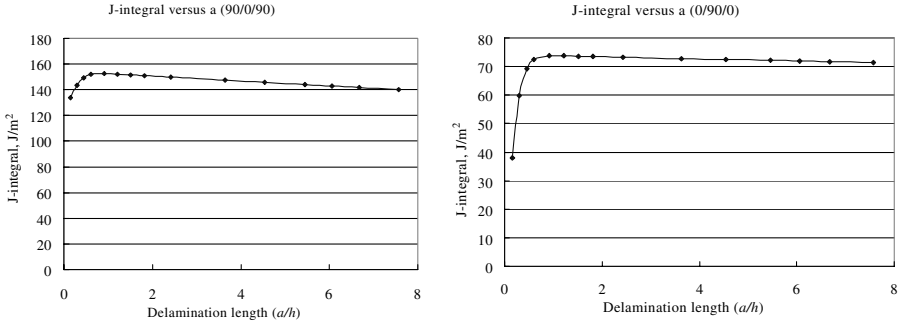


**a) [90/0/90] laminate** **b) [0/90/0] laminate**

**Fig. 4 J-integral variation with respect to delamination length $a$, which is normalized by dividing by ply thickness $h$.**

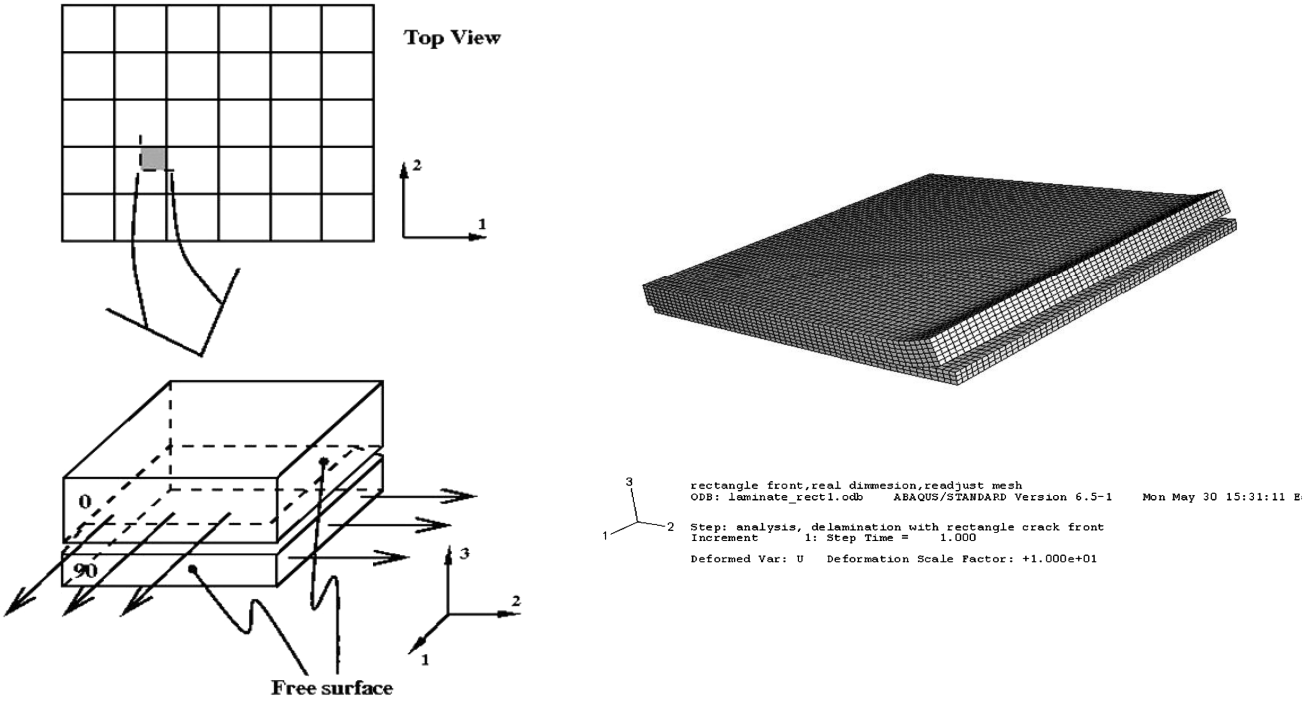


a) b)

**Fig. 5 Three-dimensional delamination model and typical deformation.**

larger than the two-dimensional result. Therefore, the local effect cannot be neglected and COD near the rectangular front should be used to compute the intersection area.

### B. Intersection Area Computation

Because of the linear relation between COD and load, the intersection area under any loading case $(N_x, N_y, \Delta T)$ can be obtained once the following three basic cases are computed:

1) $\varepsilon_x = 1\%$, $\varepsilon_y = 0$, $\Delta T = 0$

2) $\varepsilon_x = 0$, $\varepsilon_y = 1\%$, $\Delta T = 0$

3) $\varepsilon_x = 0$, $\varepsilon_y = 0$, $\Delta T = -223\ ^\circ\mathrm{C}$ (from room temperature to cryogenic temperature)

For any $(N_x, N_y, \Delta T)$, the corresponding $(\varepsilon_x, \varepsilon_y, \Delta T)$ can be obtained from the following basic formula for composite laminates, in which the matrices $[A]$ and $[\alpha]$ are determined from the preceding three basic cases:

$$\begin{Bmatrix} N_x \\ N_y \end{Bmatrix} = \begin{bmatrix} A_{11} & A_{12} \\ A_{21} & A_{22} \end{bmatrix} \left( \begin{Bmatrix} \varepsilon_x \\ \varepsilon_y \end{Bmatrix} - \Delta T \begin{Bmatrix} \alpha_x \\ \alpha_y \end{Bmatrix} \right) \tag{11}$$

and the corresponding CODs are obtained by superposing the results of three typical cases with different weighting factors. The intersection area $\Delta A$ is computed by assuming that the intersection formed by the CODs at corner is a rectangle. Figure 7 shows the variation of the intersection area, which is normalized by $h^2$, with respect to the mechanical and thermal loads. In Fig. 7a, different marks represent different ratios between $N_y$ and $N_x$, the solid lines represent the cases with thermal load and the dotted lines represent without thermal load; in Fig. 7b, each surface represents the intersection area variation with respect to $N_y$ and $N_x$ under certain thermal load.

Actually, from those three basic numerical tests, the CODs can be expressed explicitly in terms of $N_x$, $N_y$, and $\Delta T$.

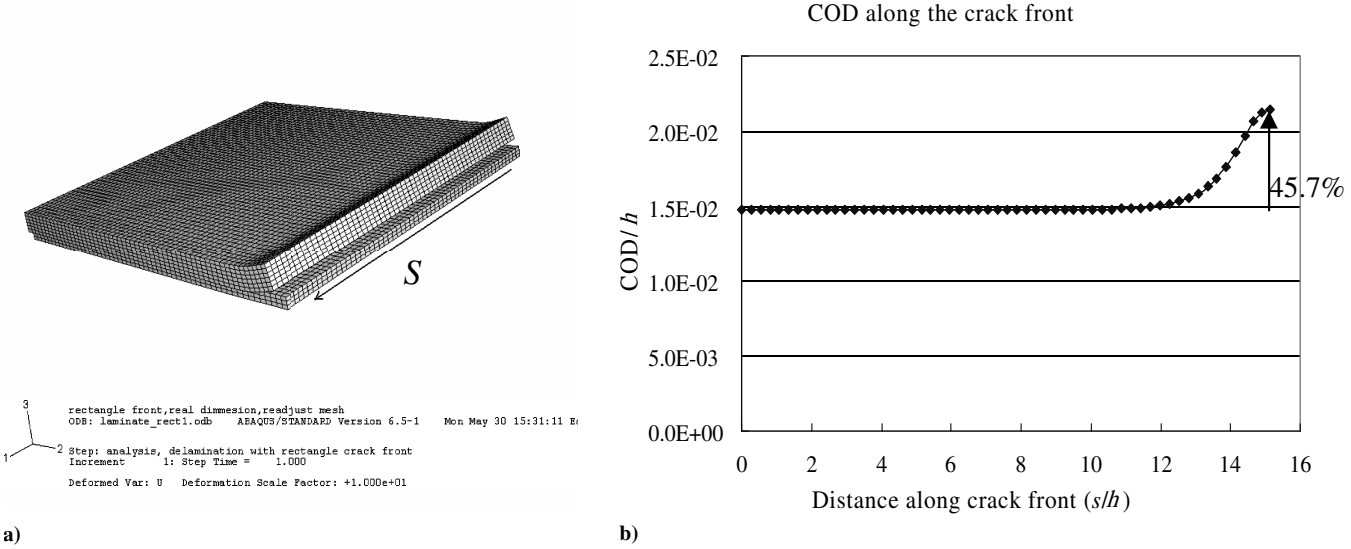


a) b)

**Fig. 6 COD along the crack front shows the local effect.**

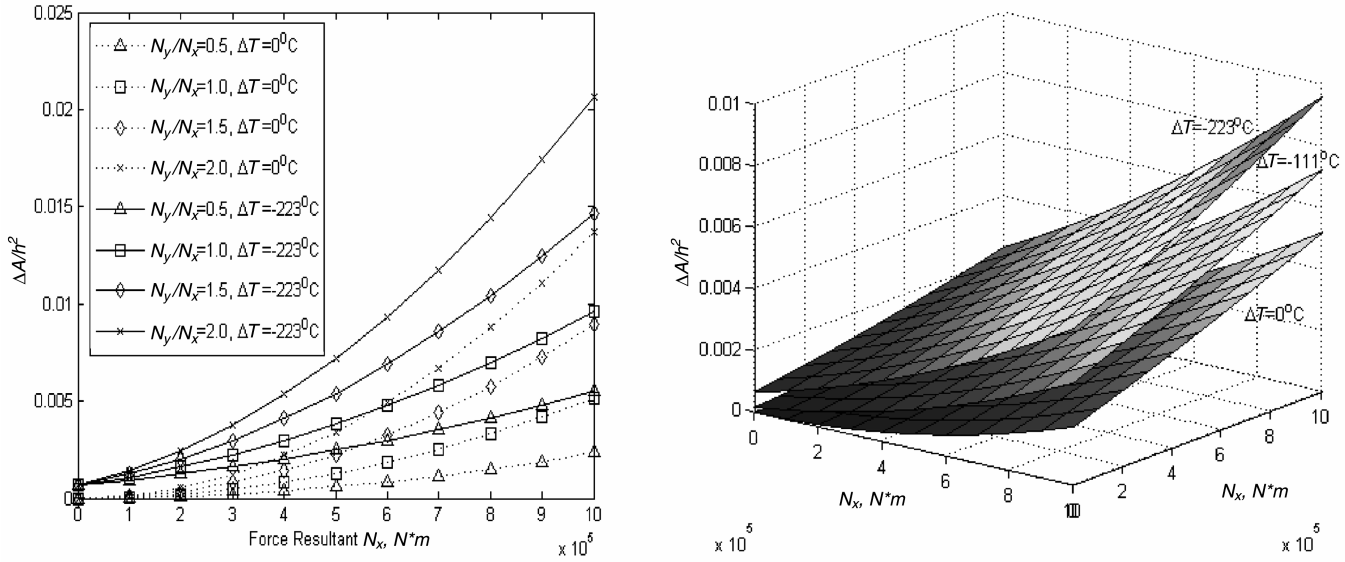


a) b)

**Fig. 7 Variation of intersection area with respect to $N_x$, $N_y$, and $\Delta T$.**

$$\Delta u = 0.592e^{-11}N_x + 0.446e^{-11}N_y - 1.082e^{-8}\Delta T \tag{12}$$

$$\Delta v = 0.204e^{-11}N_x + 1.156e^{-11}N_y - 1.036e^{-8}\Delta T \tag{13}$$

The corresponding intersection area $\Delta A$ is given by

$$\Delta A = 4 \times \Delta u \times \Delta v = 0.121e^{-22}N_x^2 + 0.516e^{-22}N_y^2 + 0.112e^{-15}\Delta T^2 + 0.775e^{-22}N_xN_y - 0.834e^{-19}N_x\Delta T - 0.171e^{-18}N_y\Delta T \tag{14}$$

From Eq. (14), the intersection area shows parabolic variations with respect to $N_x$, $N_y$, and $\Delta T$, which can be seen clearly in Fig. 7. Equations (12–14), however, are only valid for the current model. If any condition of the model, such as delamination length, material properties, and ply thickness, is changed, we have to repeat those three numerical tests.

### C. Effects of Delamination Shape and Delamination Length

The effects of delamination shape and the delamination length on the intersection area are investigated in this section. Previously, the interlaminar delamination fronts developed from 0-deg plies and from 90-deg plies were connected by a pair of straight lines forming a rectangular delamination front. However, if three-dimensional J-integrals are computed along the crack front as shown in Fig. 8, it can be seen that the highest value occurs at the corner, that is, the crack will first propagate at the corner. Hence, the delamination with a circular front might be a more appropriate scenario. Figure 8a shows the top view of the delamination and Fig. 8b shows the distribution of J-integral with different connection. The model is subjected to thermal load only. As we can see, the J-integral value remains constant at the straight crack front and increases near the corner. For the case of rectangular front, the J-integral value computed at the corner, which is extremely high due to the discontinuity of first-order derivative, may not be meaningful and is eliminated from Fig. 8b. As we expected, the circular delamination front reduces the highest value of the J-integral at corner and the bigger the radius, the lower the value. Figure 9a shows the effects of the radius of the connecting circle. In all three basic cases, the intersection area varies quadratically with the radius.

Moreover, the effect of delamination length is also investigated, as shown in Fig. 9b. In this case, the rectangular front is still used and the delamination length changed from half of the ply thickness to twice the ply thickness. It can be seen that the intersection area is more sensitive to the delamination length than to the circle radius. It does not show the tendency to reach a plateau as mentioned by Roy and Benjamin [8].

### D. Delamination Only from the Surface Ply

Another phenomenon shown in Fig. 8b is that the steady-state values along two different straight crack fronts are quite different even though both directions are under the same loading condition. Hence, delaminating from the surface ply (high J-integral) is much easier to happen than delaminating from the middle ply (low J-integral). From different views of the typical deformation of unit cell

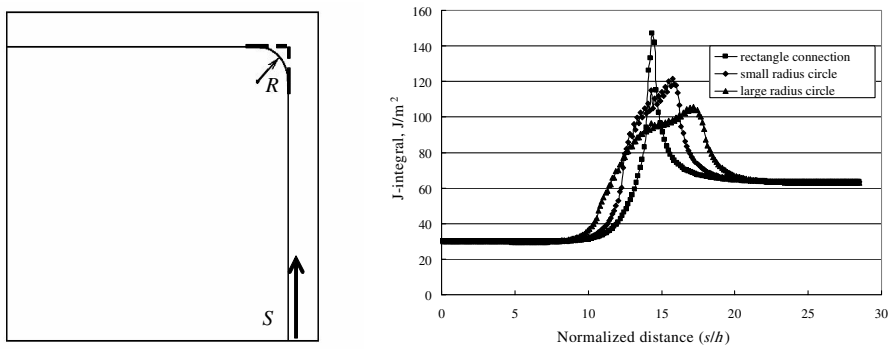


a) b)

**Fig. 8 J-integral distribution along crack front with different connect radius.**

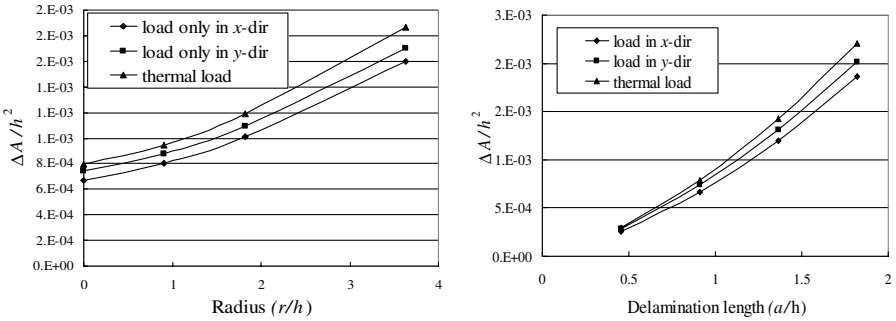


a) b)

**Fig. 9 Effect of the delamination shape and delamination length on the intersection area.**

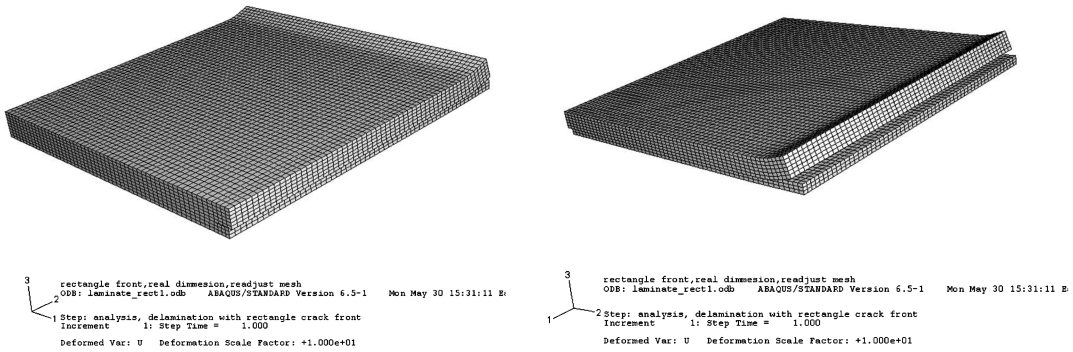


a) b)

**Fig. 10 Typical deformation of unit cell from different views.**

as shown in Fig. 10, it can be seen that delamination from middle ply (Fig. 10a) tries to close, whereas the delamination from surface ply (Fig. 10b) tries to open up. Therefore, it is much possible that delamination only emanates from surface plies. Even if delamination appears on only one side, the path for gas leakage can still be formed as shown in Fig. 11.

In this case, the intersection area is smaller than that in the previous model. Figure 12 shows the comparison between two different scenarios under the same loading condition ($N_y/N_x = 0.5$ and $\Delta T = -223°\text{C}$). The intersection area $\Delta A$ in the current scenario (single delamination) also shows a parabolic variation, but the magnitude is only about half of that in the previous model (pair of delaminations).

### E. Effect of Layups

Till now, only three-ply laminates are investigated. In reality, there are various layup possibilities. Choi [5] did permeability tests for different laminates and found that for the same thickness the specimen with layers grouped together has higher permeability than the one with layers dispersed, that is, $[0/90/0_2/90/0]_T$ performs better than $[0_2/90_2/0_2]_T$. In this section, current modeling technique will be used to investigate the effect of the layups on the permeability. In this investigation, layup $[0/90/0_2/90/0]_T$ and $[0_2/90_2/0_2]_T$ are used. For the specimen $[0_2/90_2/0_2]_T$, the numerical model is kept same as the one described in Sec. IV.A. For the specimen $[0/90/0_2/90/0]_T$, to describe the unit cell, the microcracks in the 0-deg plies and in 90-deg plies are assumed to appear in the same position, as shown in Fig. 13a. Because of the symmetry of the model, only one eighth of the unit cell is considered. Figure 13b shows the typical deformation of the unit cell.

The normalized permeability $B_0/C$, computed from Eq. (10), for $[0_2/90_2/0_2]_T$ is $1.26 \times 10^{-8}$ and for $[0/90/0_2/90/0]_T$ is

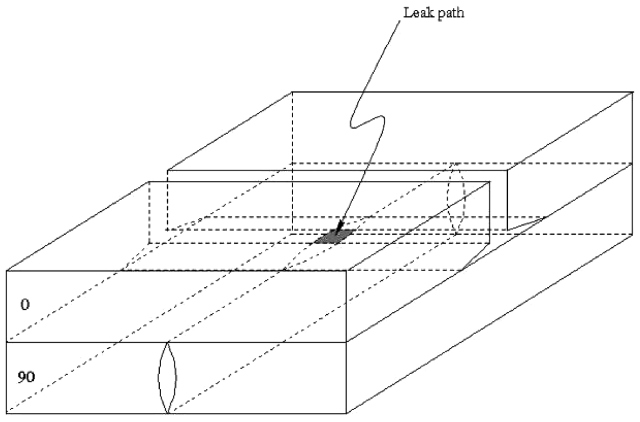


**Fig. 11 Gas leakage path formed by the delamination from the surface ply only.**

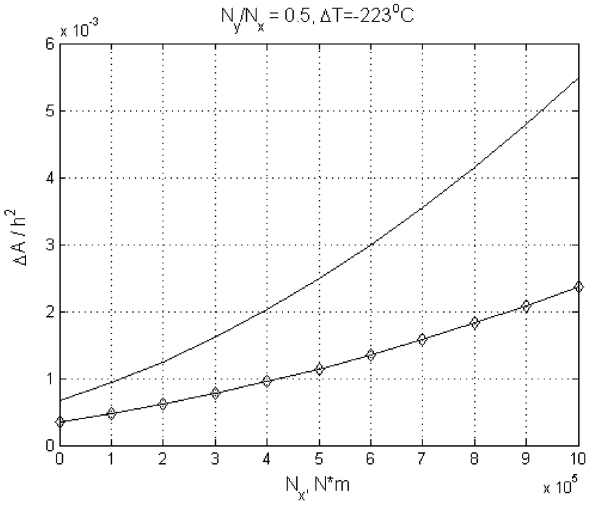


**Fig. 12 Comparison between two different scenarios.**

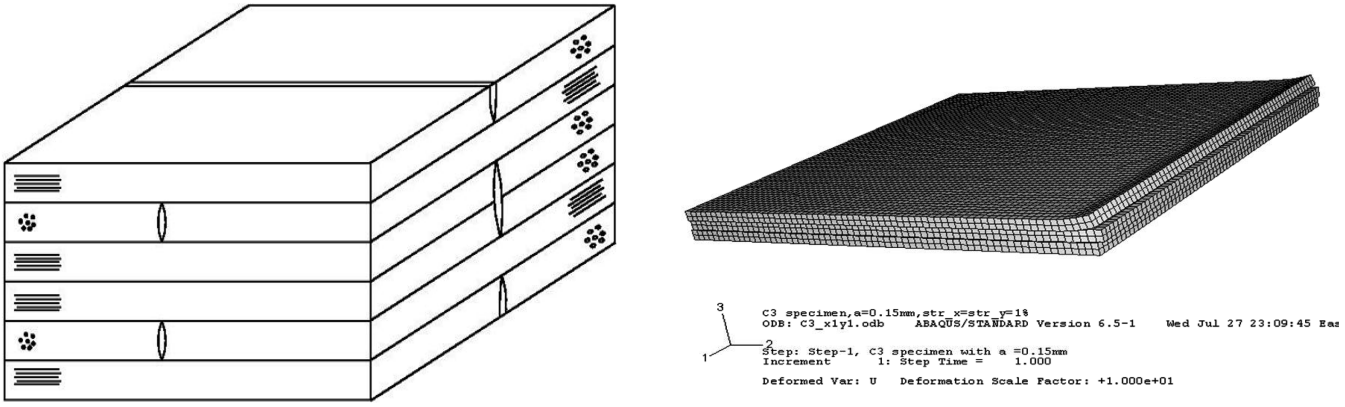


a) b)

**Fig. 13 Geometric model and typical deformation for multiple-layer laminates.**

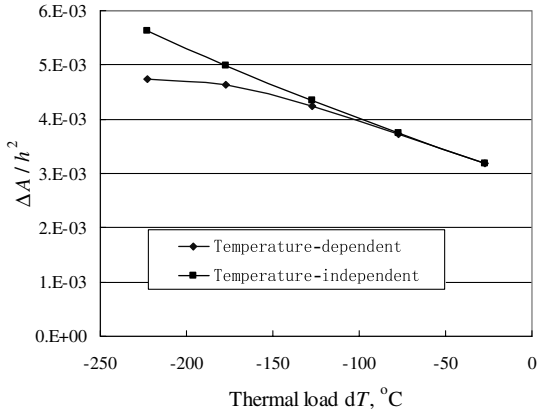


**Fig. 14 Effect of temperature-dependent material properties on the intersection area.**

$3.30 \times 10^{-9}$. It can be seen clearly that the grouped specimen has a much higher permeability than the dispersed specimen with same crack densities and under same loading case. In Choi's [5] tests, both specimens were tested at room temperature after certain cryogenic cycles (cooling the specimen down to cryogenic temperature and then warming it up to room temperature is defined as one cryogenic cycle) without mechanical loading and the crack densities in the specimens were not measured. Hence the modeling procedure does not precisely reflect the testing procedure and the modeling results are not comparable with Choi's test results. However, one fact can be confirmed from both experiments and modeling: that for the laminates with same number of plies and under similar loading conditions, the laminate with dispersed plies has lower permeability than the one with grouped plies.

### F. Temperature-Dependent Properties

In preceding sections all material properties are assumed to be temperature independent. For graphite/epoxy composite laminates, the matrix properties largely depend on the temperature whereas the fiber properties do not. Hence, the composite properties that depend mainly on matrix properties, such as transverse modulus $E_2$ and shear modulus $G_{12}$, vary remarkably with respect to temperature. Schulz [12] and Speriatu [13] performed experiments to measure the temperature-dependent properties of graphite/epoxy composite IM7/977-2. Transverse modulus $E_2$, shear modulus $G_{12}$, and coefficient of thermal expansion $\alpha$ are measured and fitted with polynomial functions. In the following simulation, these experimental results are used. Longitudinal modulus $E_1$ and Poisson's ratios are assumed to be constants, and shear modulus $G_{23}$ is assumed to follow the relation

$$G_{23} = \frac{E_2}{2(1+\nu_{23})} \tag{15}$$

In the simulation, constant strain boundary conditions are applied. Strains in both $x$ direction and $y$ direction are 1%. Thermal load is applied from room temperature to cryogenic temperature. Figure 14 shows the simulation results. The line with square marks is the result with temperature-independent material properties and the line with diamond marks is the result with temperature-dependent properties. From this figure, it can be seen that at cryogenic temperature the result with temperature-dependent properties is almost 15% less than the one with temperature-independent properties. Hence, if temperature-independent material properties are adopted, the simulation will give the upper bound of the permeability.

## V. Conclusions

In the present work, the gas permeability of symmetric cross-ply laminates subjected to biaxial and thermal loading is investigated in detail using FE modeling. Based on Darcy's law for porous materials, the permeability is determined from the crack density, intersection area formed by crack opening displacements, and a material constant to be determined from experiments. The research focused on determining the intersection area available for gas leakage. The following conclusions are reached from the results:

1) Local effects on crack opening displacements are not negligible.

2) The intersection area for a given model under any arbitrary loading condition can be obtained from three basic numerical simulations.

3) The intersection area is strongly influenced by delamination shape and delamination length.

4) Leakage path can still be formed in [0/90/0] laminate if delamination only occurs from the surface ply.

5) For a given laminate thickness, the laminates with dispersed layers show lower permeability than the laminates with grouped layers.

6) Although some of the composite properties depend strongly on the temperature, temperature-independent material properties give the upper bound for the laminate permeability.

The results from this study will be useful in understanding how various factors will affect the gas permeability, and thus provides both qualitative and quantitative guidance to the design of laminates for cryogenic storage applications.

## Acknowledgment

The authors gratefully acknowledge the technical and financial support of NASA John H. Glenn Research Center (NAG3-2750) and NASA Kennedy Space Center under the Hydrogen Research and Education Program.

## References


[1] ASTM D1434-82 (Reapproved 1992), "Standard Test Method for Determining Gas Permeability Characteristics of Plastic Film and Sheeting," American Society for Testing and Materials Paper 203-213, 1992.

[2] Stokes, E., "Hydrogen Permeability of Polymer Based Composite Tank Material Under Tetra-Axial Strain," *Proceedings of the Fifth Conference on Aerospace Materials, Processes and Environment Technology (AMPET)*, Southern Research Institute, Birmingham, AL, Sept. 2002.

[3] Nettles, A. T., "Permeability Testing of Impacted Composite Laminates for Use on Reusable Launch Vehicles," NASA TM-2001-210799, 2001.

[4] McManus, H. L., Faust, A., and Uebelhart, S., "Gas Permeability of Thermally Cycled Graphite-epoxy Composites," American Society for Composites, Paper 092, Blacksburg, VA, Sept. 2001.

[5] Choi, S., "Micromechanics, Fracture Mechanics and Gas Permeability of Composite Laminates for Cryogenic Storage Systems," Ph.D. Dissertation, Univ. of Florida, Gainesville, FL, 2005.

[6] Kumazawa, H., Aoki, T., and Susuki, I., "Analysis and Experiment of Gas Leakage Through Composite Laminates for Propellant Tanks," *AIAA Journal*, Vol. 41, No. 10, Oct. 2003, pp. 2037–2044.

[7] Berthelot, J.-M., "Transverse Cracking and Delamination in Cross-Ply Glass-Fiber and Carbon-Fiber Reinforced Plastic Laminates: Static and Fatigue Loading," *Applied Mechanics Reviews*, Vol. 56, No. 1, Jan. 2003, pp. 111–147.

[8] Roy, S., and Benjamin, M., "Modeling of Permeation and Damage in Graphite-Epoxy Laminates for Cryogenic Fuel Storage," *Composites Science and Technology*, Vol. 64, Nos. 13–14, 2004, pp. 2051–2065.

[9] Kulichenko, A. V., "Theoretical Analysis, Calculation, and Prediction of the Air Permeability of Textiles," *Fibre Chemistry*, Vol. 37, No. 5, 2005, pp. 371–380.

[10] Bapanapalli, S. K., Sankar, B. V., and Primas, R. J., "Microcracking of Symmetric Cross-Ply Laminates Subjected to Biaxial Loading," AIAA Paper 2005-2230, April 2005.

[11] Sun, C. T., and Jih, C. J., "On Strain Energy Release Rate for Interfacial Cracks in Bimaterial Media," *Engineering Fracture Mechanics*, Vol. 28, No. 1, 1987, pp. 13–20.

[12] Schulz, W. A., "Determination of Residual Stress and Thermal Behavior for Composite Laminates," M.S. Thesis, Univ. of Florida, Gainesville, FL, 2005.

[13] Speriatu, L. M., "Temperature Dependent Mechanical Properties of Composite Materials and Uncertainties in Experimental Measurements," Ph.D. Dissertation, Univ. of Florida, Gainesville, FL, 2005.


A. Berman
*Associate Editor*